HYBRID WELDING OF ALUMINIUM 1561 AND 5083 ALLOYS USING PLASMA-ARC AND CONSUMABLE ELECTRODE ARC (PLASMA-MIG)

O.A. Babych[1], **V.M. Korzhyk**[1,2], **A.A. Grynyuk**[2], **V.Yu. Khaskin**[1,2], **Chunlin Dong**[1] and **Shanguo Han**[1]

[1]Guangdong Institute of Welding (China-Ukraine E.O. Paton Institute of Welding)
363 Chiansin Str., 510650, Guangzhou, Tianhe
[2]E.O. Paton Electric Welding Institute of the NAS of Ukraine
11 Kazymyr Malevych Str., 03150, Kyiv, Ukraine. E-mail: office@paton.kiev.ua

In the article it is shown that to improve mechanical properties and decrease indices of stress-strain state of welded joints of alloyed aluminium 1561 and 5083 alloys it is rational to apply hybrid plasma-arc welding using arc of the consumable electrode, which as compared to traditional welding using arc of the consumable electrode allows reducing the electrode wire consumption by 10−30 %, input energy — up to 25 %, residual deformations — by 2−3 times, residual stresses — by about 20 % according to the absolute values, as well as reducing burnout of such alloying element as Mg by 15−20 %. 19 Ref., 6 Tables, 9 Figures.

K e y w o r d s : hybrid plasma-arc welding using consumable electrode (Plasma-MIG), pulsed-arc welding using consumable electrode (MIG), surfacing welds, butt welds, strength, burnout of alloying elements, stress-strain state

The intensive development of land, air and sea high-speed transport necessitates the use of innovative high-performance technologies for producing welded joints of aluminium alloys. This is associated with a number of drawbacks inherent in traditional welding processes. Thus, in the case of using consumable electrode arc welding (MIG welding) a significant overheating of the electrode metal occurs, which leads to a partial burnout of alloying elements of aluminium alloys and, as the consequence, a decrease in the strength of the produced joints. In addition, during MIG welding fairly wide welds are formed and significant residual deformations occur. In the case of welding using nonconsumable electrode arc (TIG welding), the efficiency is reduced and significant residual deformations also occur. Producing welded joints is complicated by the fact that the processes of MIG and TIG welding require a preliminary preparation of edges to be welded.

One of the ways to eliminate the mentioned problems is the use of plasma welding. However, this process also has some drawbacks. First, the melting of the filler wire requires additional energy, the consumption of which leads to an increase in the input energy of welding. This can lead to the formation of certain residual stresses (deformations). Secondly, the increased energy intensity and axial concentration of pressure (phenomenon of keyhole formation) lead to

the defects of welds formation (in particular, undercuts, root defects, nonuniform formation of upper reinforcement bead) and the presence of inner porosity.

In the last decade, traditional problems of welding and related technologies are solved through the use of hybrid technologies [1]. Difficulties in producing joints of alloyed high-strength aluminium alloys are also solved by a hybrid combination of the advantages of plasma and arc welding methods. For this purpose in one welding pool the energy of the constricted arc with nonconsumable and an arc with the consumable electrode is concentrated. Such an approach allows narrowing the weld and reducing (or completely eliminate) the need in preparation of edges to be welded. It also increases the efficiency of welding by stabilizing the action of the arc of the consumable electrode by influencing the plasma-arc, which covers the first outside. All this makes the application of the technology of hybrid plasma-arc welding using the consumable electrode, better known in the world as Plasma-MIG, relevant.

The process of plasma-arc welding with the consumable electrode including for joining of aluminium alloys was developed in the 1970s by a group of researchers from the laboratory of the Philips Company [2]. Due to certain difficulties in creating the optimal design of the torch and power sources adapted namely for this process, hybrid Plasma-MIG welding still has some limita-

O.A. Babych — https://orcid.org/0000-0001-5633-5721, V.M. Korzhyk — https://orcid.org/0000-0001-9106-8593,
A.A. Grynyuk — https://orcid.org/0000-0002-6088-7980, V.Yu. Khaskin — https://orcid.org/0000-0003-3072-6761,
Chunlin Dong — https://orcid.org/0000-0003-2672-5985, Shanguo Han — https://orcid.org/0000-0002-4299-9786

tions in industrial application. For example, it should be taken into account that in this type of hybrid process the arc of the consumable electrode exists in the environment of ionized argon plasma generated by the arc of the nonconsumable electrode, which radically changes the conditions of its burning as compared to GMAW/MIG process. In [3], it was shown that electrical conductivity of the external arc is significantly higher than that of the inner arc due to the higher density of electrons. Respectively, most of the current between the consumable electrode and the base metal flows through the outer arc, and to the inner arc about 5 % of the current goes. This is also confirmed by the higher glow of the outer arc in the area below the end of the consumable electrode. The higher intensity of glow of the inner arc as compared to the outer one, which is noted by most researchers, is predetermined not by the high glow density of current flowing through it, but by a higher glow intensity of the elements that are a part of the gas phase in this area.

At present, active investigations of the process of hybrid plasma-arc welding using consumable electrode continue. Such investigations are carried out at a number of universities, in particular, at the Chemnitz University of Technology and in SLV Muenchen (Germany) [4, 5]. The similar investigations are carried out at the Perm State University (Russia) [6, 7]. The peculiarities of the process of plasma-arc welding using consumable electrode were also studied in China, Japan, and Brazil [8, 9]. In Ukraine, the issues of plasma-arc welding using consumable electrode were undertaken at the Pre-Azov State Technical University and the E.O. Paton Electric Welding Institute of the NASU [10].

The investigations carried out in the last decade were aimed at a thorough study of separate components of the process and its behavior in general. In [11], it was shown that during welding of aluminium alloys with an increased electrode wire feed rate, the size of undercuts decreases as the amount of welding wire in the welding pool increases. Increasing the diameter of the plasma-forming nozzle also facilitates the elimination of undercuts because of a low electromagnetic stirring force caused by a low density of plasma current. However, the increase in the wire feed rate and, accordingly, the arc current of the consumable electrode, shifts the process towards the traditional MIG welding, which eliminates the advantages of the hybrid method. Reduction in the plasma current density can contribute to arising spattering of the metal by the arc of the consumable electrode. In [10, 12] the peculiarities of the behavior of both electric arcs, their influence on each other, on the formation

of a liquid metal drop and the process of mass transfer were studied quite deeply.

The model of heating the electrode wire in the process of hybrid plasma-arc welding using consumable electrode (Plasma-MIG) proposed in [12] allowed carrying out a preliminary evaluation of the plasma temperature of an integrated gas discharge. During welding of aluminium alloys with a thickness of 5−12 mm, it can be about 7300−7400 K. This indicates the danger of burnout low-melting alloying elements that are a part of the electrode wire and the base metal, which can lead to weakening of the produced joints. In addition, in [12] a tendency of increasing the voltage on the arc of the nonconsumable electrode with an increased flow rate of the plasma-forming gas and its temperature is observed. Such a feature of the hybrid process should be taken into account when selecting welding modes, in particular, optimizing the power ratio of plasma and arc components.

In contrast to the previously published works, this paper pays attention to the influence of the hybrid Plasma-MIG process modes on the geometry and stress-strain state of the produced joints, as well as its comparison with a traditional pulsed-arc welding process. In this case, producing high-quality joints is planned due to a concomitant preheating of welded metal by a plasma-arc and reducing the arc voltage of the consumable electrode with a simultaneous increase in its penetration into the metal. It is expected that the mutual influence of the components of the hybrid welding process can contribute to the reduction of input energy and the share of burnout of alloying elements.

The aim of the investigation is to improve the mechanical properties and reduce the stress-strain state of welded joints of alloyed aluminium alloys by reducing the amount of the used electrode wire, input energy and burnout of alloying elements due to the use of hybrid plasma-arc welding.

Achieving this aim was carried out accoding to the following procedure. At first, on the basis of the literature data, the intervals of varying parameters of the modes of hybrid plasma-arc (Plasma-MIG) welding were selected. Then, applying mathematical modeling, the influence of these parameters on the penetration depth and welding speed was analyzed, and then the most promising parameters from the standpoint of minimizing heat input and energy input were selected. The reliability of the calculations was checked and on the selected modes welding of the test specimens was performed. Moreover, the mutual influence of the plasma-arc and the arc of the consumable electrode on each other, as well as their joint influence on the hybrid welding process were analyzed. To compare

Table 1 Chemical composition of aluminium 5083 and 1561 alloys and electrode wire ER5356, wt.%

Grade of alloy	Fe	Si	Mn	Cr	Ti	Al	Cu	Be	Mg	Zn	Impurities
5083	≤0.4	≤0.4	0.4−1.0	0.05−0.25	≤0.15	Base	≤0.1	≤0.005	4.0−4.9	≤0.25	≤0.15
1561	≤0.4	≤0.4	0.7−1.1	–	–	Same	≤0.1	0.0001−0.003	5.5−6.5	≤0.2	≤0.1
ER5356	0.1−0.2	0.08	0.12	0.13	0.13	»	0.02	–	4.95	≤0.02	–

Table 2 Generalized thermophysical characteristics of aluminium alloys under normal conditions

Density ρ, kg/m³	Specific heat capacitance, J/(kg °C)	Coefficient of thermal conductivity λ, W/(m·°C)	Coefficient of thermal conductivity a, m²/s	Specific heat of melting L, kJ/kg	Specific heat of evaporation E, kJ/kg	Melting point, T_{m}, K	Temperature of beginning of phase transitions, K
2640	922	122	$5.0122 \cdot 10^{-5}$	390	10530	660	460

the obtained results, traditional pulsed-arc welding of similar specimens was performed at the same speed or as close as possible to the input energy. Mechanical tests of the produced specimens were conducted. The burnout of one of the most volatile alloying elements (magnesium) in welding processes was investigated. The stress-strain state of the welded specimens was investigated. Based on the obtained results, the appropriate conclusions were made.

To perform preliminary technological calculations in terms of the widest application in industrial welded structures, the aluminium alloys 5083 and 1561 were selected, during welding of which the electrode wire ER5356 is used (Table 1). To simplify the evaluation calculations, the generalized thermophysical characteristics of these alloys were used, given in Table 2.

To model the heat source operating during Plasma-MIG welding in the aluminium plate, the model of J. Goldak [13] was used (Figure 1). According to this model, the heat source was represented as a double ellipsoid. The calculation of the considered thermal welding processes was performed using finite element modeling. As a basic assumption, it was assumed that an unlimited plate of aluminium alloy with a thickness δ (for example, δ = 10 mm) is welded by a surfacing weld. In this case, the volume of the metal introduced by the consumable electrode was taken into account as the volume of the metal of the plate to be welded, remelted by the arc of this electrode. To increase the accuracy of calculations in the area of the heat source, a grid with a smaller step was used, and in other areas — with a relatively large step.

The finite element method used in the calculations is based on the assumption that a body can be represented as a set of elements connected to each other only in nodes. The relationship of nodal changes in temperature over time is set by the temperature matrix of the element. Combining the temperature matrices of separate elements into a global temperature matrix

of a body allows recording the conditions of a thermal equilibrium of a body as follows:

$$C(T)\rho(T)\frac{\partial T}{\partial t} = \frac{\partial}{\partial x}\left(\lambda(T)\frac{\partial T}{\partial x}\right) + \frac{\partial}{\partial y}\left(\lambda(T)\frac{\partial T}{\partial y}\right) +$$
$$+ \frac{\partial}{\partial z}\left(\lambda(T)\frac{\partial T}{\partial z}\right), \ 0 < z <, \ t > 0, \tag{1}$$

where $C(T)$, $\rho(T)$, $\lambda(T)$ is the effective heat capacity of the metal (taking into account the latent heat of fusion), density and thermal conductivity coefficient, respectively; x, y, z are the Cartesian coordinates (heat source moves along the coordinate x at a speed V); δ is the thickness of the metal plate to be welded; t is the time coordinate.

At set temperatures, the action of which changes over time, and at a known global temperature matrix, the solution of the system of equations of thermal equilibrium (balance) allows finding all the nodal values of temperature depending on the time of the heat source, and using the latter — temporary temperature changes within each element. This is how the spatial-temporal distribution of body temperatures was determined [14].

On the surface of the plate, which is heated by a hybrid plasma-arc heat flux $q(t)$ over time t, a volumetric heat source with a radius R_{PL} is formed, which contains a second heat source with a slightly smaller
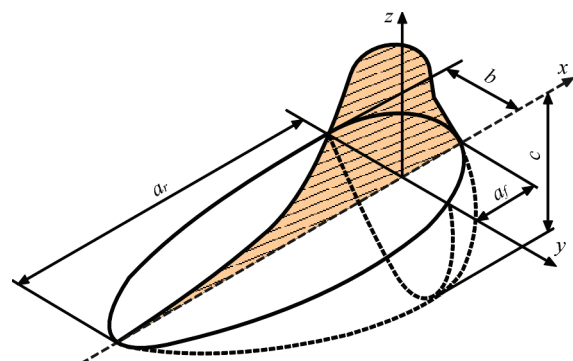
Figure 1 Scheme of model of distributed volumetric heat source, which has a shape of a double ellipsoid [13]

radius R_{MIG}. In the process of Plasma-MIG welding, at the set point on the surface, at first it will be heated by the plasma source and then by the sum of the arc (MIG) and plasma sources, and finally by the plasma source again. The constant of time (time of influence of the heat source) in each of these three cases will be:
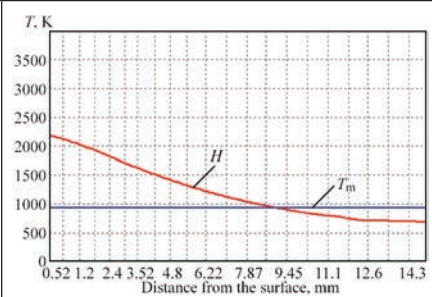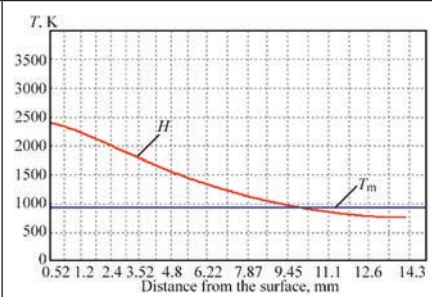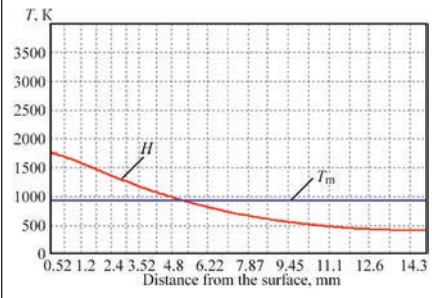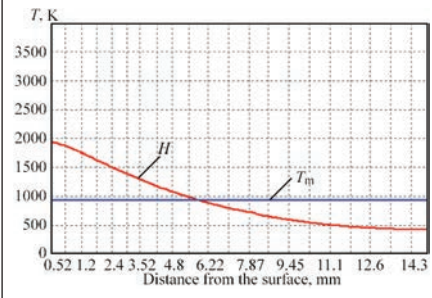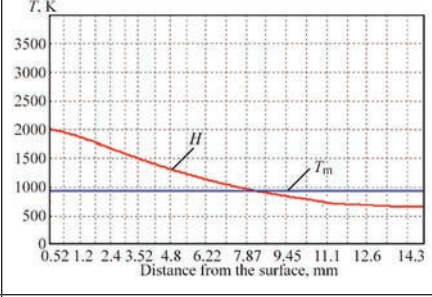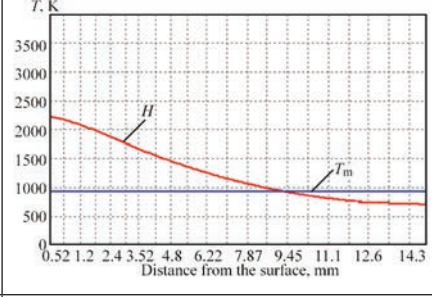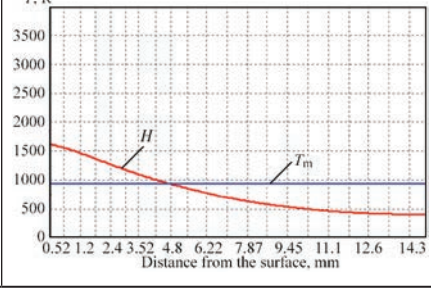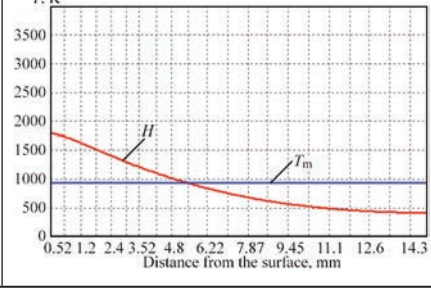
$$t_1 = \frac{R_{PL} - R_{MIG}}{V} \; ; \; t_2 = t_1 + \frac{2R_{MIG}}{V} \; ; \; t_3 = t_2 + t_1. \quad (2)$$

Then on the plate to be welded a heat flux will act

$$q_\Sigma (t) \begin{cases} q_{PL}, \, 0 < t < t_1 \\ q_{PL} + q_{MIG}, t_1 < t < t_2 \\ q_{PL}, \quad t_2 < t < t_3 \end{cases} ; \quad (3)$$

where $q_{MIG} = A(T)\dfrac{P_{MIG}}{\pi R_{MIG}^2}$ is the heat flux introduced by the arc of the consumable electrode (MIG), $q_{PL} = A(T)\dfrac{P_{PL}}{\pi R_{PL}^2}$ is the heat flux introduced by the arc plasma. Such heat fluxes are created in the plate to

Table 3 Results of calculated determination of height of welds H and constant of time τ, which are obtained during Plasma-MIG welding of aluminium 5083 and 1561 alloys

Mode parameters	Results				
	Welding speed 10.0 mm/s		$H,$ mm/τ, s	Welding speed 16.7 mm/s		$H,$ mm/τ, s
	Dependence $H = f(T)$			Dependence $H = f(T)$		
$P_{MIG} \approx 4000$ W, $P_{PL} \approx 5000$ W, $d_{MIG} = 10.0$ mm, $d_{PL} = 11.5$ mm			$H = 9.0$ mm/ $\tau = 1.18$ s			$H = 5.2$ mm/ $\tau = 0.694$ s
$P_{MIG} \approx 4000$ W, $P_{PL} \approx 4000$ W, $d_{MIG} = 10.0$ mm, $d_{PL} = 11.5$ mm			$H = 8.2$ mm/ $\tau = 1.18$ s			$H = 4.7$ mm/ $\tau = 0.694$ s
$P_{MIG} \approx 5000$ W, $P_{PL} \approx 5000$ W, $d_{MIG} = 10.0$ mm, $d_{PL} = 11.5$ mm			$H = 9.9$ mm/ $\tau = 1.18$ s			$H = 5.8$ mm/ $\tau = 0.694$ s
$P_{MIG} \approx 5000$ W, $P_{PL} \approx 4000$ W, $d_{MIG} = 10.0$ mm, $d_{PL} = 11.5$ mm			$H = 9.3$ mm/ $\tau = 1.18$ s			$H = 5.4$ mm/ $\tau = 0.694$ s

be welded by a volumetric heat source, the shape of which is shown in Figure 1.

In the course of the computer modeling, in accordance with the recommendations of [8−12], the modes of Plasma-MIG welding processes were selected, according to which using the method of finite-element modeling, the temperature distribution in the depth in the plate to be welded was determined. By means of the time constant (τ, s) and the size of the heat source (d_{PL}, mm), the welding speed (V, mm/s) was determined. Depending on the evaluation of the temperature distribution in the depth of the plate (depending on the powers of the components of the sources P_{PL} and P_{MIG}, W), this allowed selecting the approximate parameters of the modes in which it is rational to perform welding of butt joints (Table 3).

When choosing the parameters of the Plasma-MIG welding modes, both the depth of penetration H as well as the width of the formed weld were taken into account, approximately corresponding to the parameter d_{MIG}. For welding plates with a thickness of $\delta = 10$ mm, between the edges to be butt-joined a gap was left approximately equal to the diameter of the electrode wire (i.e. ~ 1.6 mm), which allowed narrowing the weld and increase the speed of the process. Welding of plates $\delta = 5$ mm was carried out with a tight joining of edges. In all cases, welding was performed on a substrate to avoid leakage of the pool. Such technological methods in combination with calculated forecasts allow choosing the welding speed of 16.7 mm/s (60 m/h). In this case, in order to avoid an excessive amount of molten metal in the welding pool, the parameters of power variation should approach the ratio $P_{MIG}:P_{PL} \sim 4000:5000$ W. For example, the arc current of the consumable electrode may be $I_{MIG} = 200$ A at an arc voltage of $U_{MIG} = 20$ V, and the current of the plasma-arc $I_{PL} = 160–180$ A at $U_{PL} = 30$ V.

For experimental verification of the proposed modes, as well as for studying the technological features of Plasma-MIG welding, a laboratory model of the technological complex was designed (Figures 2, 3). When designing the equipment, the specialists focused on welding sheets of aluminium alloys with a thickness from 5 to 10 mm. According to the calculations, the total current load for this purpose should not exceed 500 A. To obtain equal opportunities to study the impact on the process of both the plasma-arc as well as the arc of the consumable electrode, the current load should be divided approximately equally. Based on this assumption, the welding power sources were selected (Tetrix 421 AC/DC of the EWM Company for the arc of the nonconsumable electrode and of FRONIUS TPS 450 for the arc of the consumable electrode) and the plasmatron was designed and integrated capable of withstanding currents
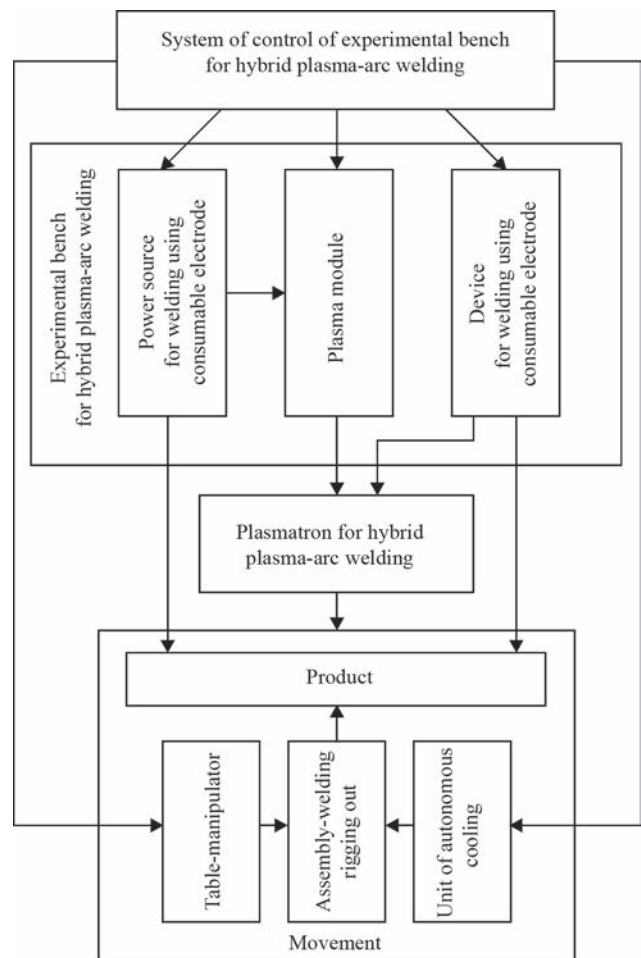

Figure 2 Block diagram of laboratory complex of Plasma-MIG welding

not less than 250 A both on the plasma-arc as well as on the arc of the consumable electrode with DC of 100 % (Figure 4). During its manufacture, the non-consumable electrode was made with a diameter of 10.0 mm with an axial hole of 5.0 mm to exclude the possibility of contact of the electrode wire of 1.6 mm diameter with the inner wall of the electrode. The diameter of the channel of the plasma-forming nozzle was selected to be equal to 10.0 mm on the grounds of approximation to the dimensions of the working plane of the nonconsumable electrode.
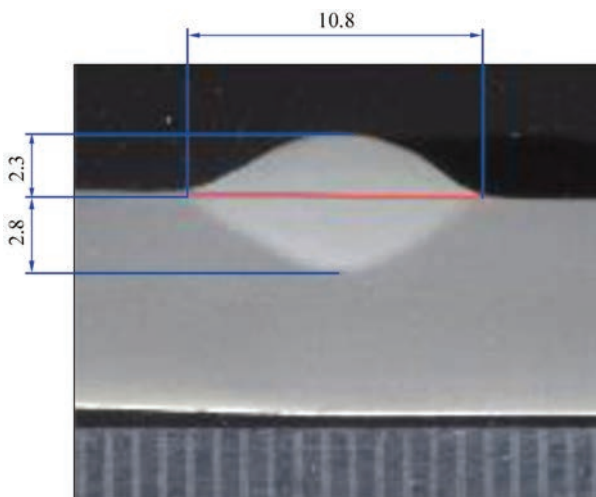

Figure 3 Appearance of laboratory complex of Plasma-MIG welding
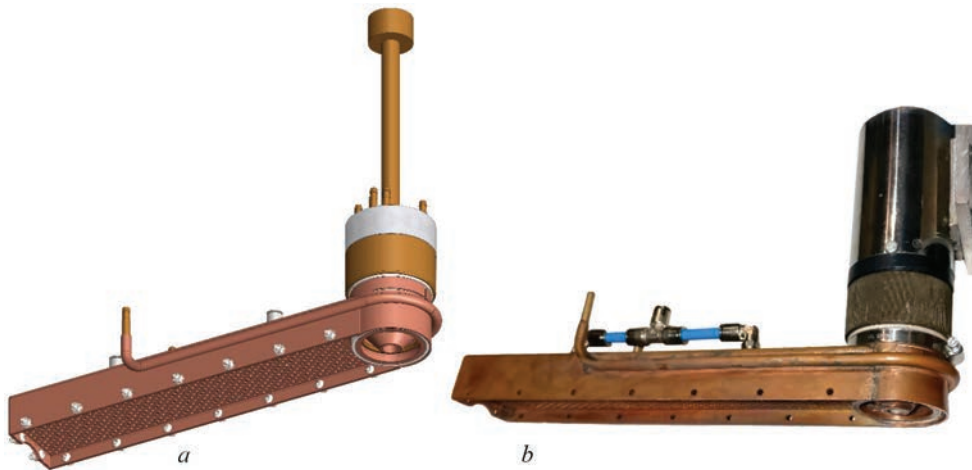
Figure 4 3D-model (*a*) and appearance (*b*) of integrated plasmatron

As specimens for experiments, the plates of aluminium 5083 and 1561 alloys with the dimensions (400−320)×(200−100)×δ mm (δ = 5.8 and 10 mm) were used. The specimens were butt-welded, also surfacing welds were produced on their surface. For welding the electrode wire ER5356 (of 1.6 mm diameter) was used.
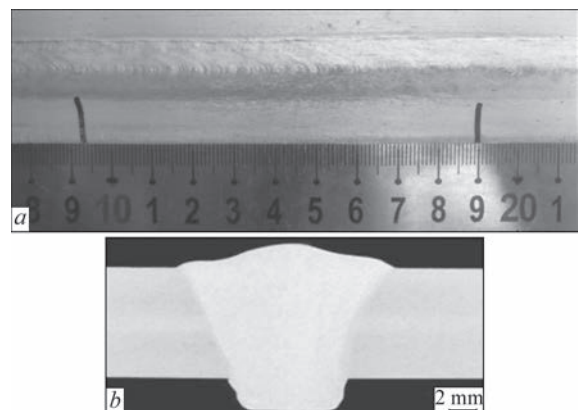
At first, a series of experiments was conducted to verify the results of calculations (Figure 5). It was found that the accuracy of the calculated value of the total height of the weld is in the range of 5−10 %, which is a satisfactory result for technological calculations. Using the modes selected by the calculation method, quality joints of 5083 alloy were produced, having a thickness of 8 and 10 mm (Figure 6). Moreover, the arc of the consumable electrode, which was constricted due to the outer plasma-arc, provided the penetration, which is close to the vapour-gas channel as to its shape without a keyhole formation, which is traditionally necessary for this.

After that, the comparative experiments on pulsed-arc welding using consumable electrode (MIG) and hybrid Plasma-MIG welding were performed (Figure 7). Here, the criterion for selecting the mode was the quality of weld formation at equal process speeds. The experiments showed a decrease in input energy by 20−25 % and a similar decrease in the width of the weld (in the example, shown in Figure 7, *a*, *b* — from 13.8 to 10.7 mm). At the same time, the integrated input energy of Plasma-MIG welding E_Σ was determined as the sum of input energies of the components of E_{MIG} and E_{PL}. Also, the experiments on Plasma-MIG welding at different speeds were carried out (for example, Figure 7, *b* and Figure 7, *c*), which showed that when the welding speed increases from 10 to 16.7 mm/s, the welds on the back side are narrowed approximately twice (for example, from 8 to 4 mm), and at the top their width remains almost unchanged. This is facilitated by a reduction in the input energy of E_Σ by ~10 % (from 530 to 480 J/mm).

To study the mutual influence of the arcs on the process of Plasma-MIG welding, a filming of the

Figure 5 Cross-section of surfacing weld produced on the plate of 1561 alloy (δ = 8 mm) at a speed of 16.7 mm/s: I_{MIG} = 200 A, U_{MIG} = 20 V, I_{PL} = 176 A, U_{PL} = 30 V


Figure 6 Appearance (*a*) and cross-section (*b*) of butt joint of 5083 alloy (δ = 8 mm), produced by Plasma-MIG welding at a speed of 6.67 mm/s: I_{MIG} = 142 A, U_{MIG} = 20 V, I_{PL} = 182 A, U_{PL} = 30 V, E_Σ ≈ 1230 J/mm

transfer of an electrode metal drop with the help of a high-speed video camera (minimum exposure time was 4 μs) was used. This made it possible to establish that the plasma-arc constricts the arc of the consumable electrode and prevents sprattering of the metal from the welding pool. The degree of constriction of the arc of the consumable electrode is directly proportional to the current of the plasma-arc. Moreover, the plasma-arc provides a concomitant heating of the weld metal, which increases the penetration depth of the arc of the consumable electrode, and also improves the formation of the upper bead. In addition, the plasma-arc heats the free end of the electrode wire and increases the uniformity of heating of the droplet that is formed in it, in comparison with the heating of a conventional arc of the consumable electrode (Figure 8). In turn, the arc of the consumable electrode contributes to the expansion of the plasma-arc. This expansion is directly proportional to the value of the arc current of the consumable electrode.

One of the important points of arc welding of aluminium alloys is the danger of burnout alloying elements of the wire and the base metal [15]. Thus, during pulsed MIG welding in argon at an increased current, the temperature of the electrode metal droplets grows (up to the temperatures of 2100−2600 K), which leads to an intensive burnout of magnesium in them (content of magnesium is 2−3 times decreased and more) [16]. Due to burnout magnesium, in the electrode metal droplets pores can be formed, which in the process of mass transfer get into the welding pool and can result in porosity of the welds. During Plasma-MIG welding, such burnout of alloying elements may be to some extent associated with the mutual influence of arcs.

This assumption was tested as follows. To obtain the investigated droplets, an instantaneous stop
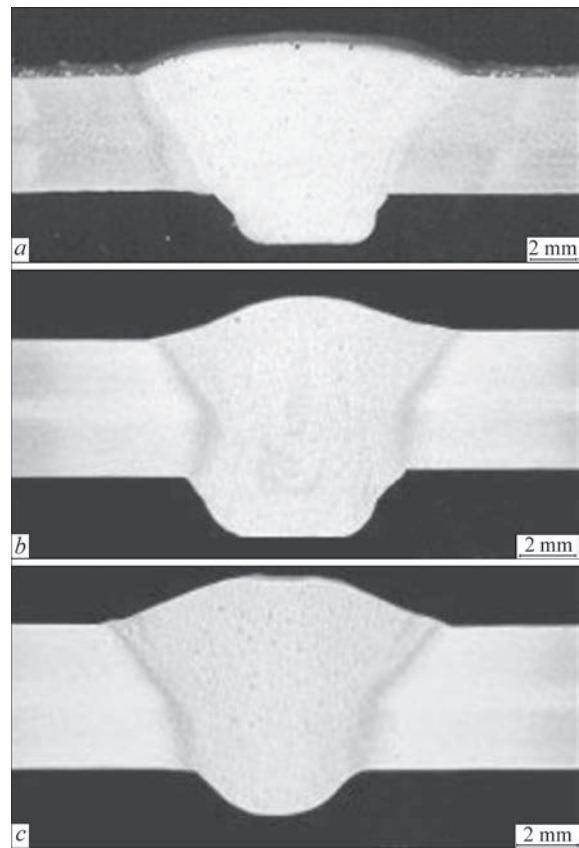

Figure 7 Cross-sections of butt joints of 1561 alloy ($\delta = 5$ mm): a — MIG welding: $V = 10$ mm/s, $I_{MIG} = 253$ A, $U_{MIG} = 26$ V, $E_{MIG} \approx 660$ J/mm; b — Plasma-MIG welding: $V = 10$ mm/s, $I_{MIG} = 165$ A, $U_{MIG} = 17.4$ V, $I_{PL} = 100$ A, $U_{PL} = 24.6$ V, $E_{\Sigma} \approx 530$ J/mm; c — Plasma-MIG welding: $V = 16.7$ mm/s, $I_{MIG} = 154$ A, $U_{MIG} = 18.2$ V, $I_{PL} = 178$ A, $U_{PL} = 29.2$ V, $E_{\Sigma} \approx 480$ J/mm

of welding was performed, which allowed the droplets to be completely formed at the free end of the electrode wire ER5356 with a diameter of 1.6 mm. To average the obtained results, 6−8 such drops were collected, which were separately investigated, applying the metallographic method (determination of porosity), and also after mechanical conglomeration — by the method of optical spectroscopy (determination
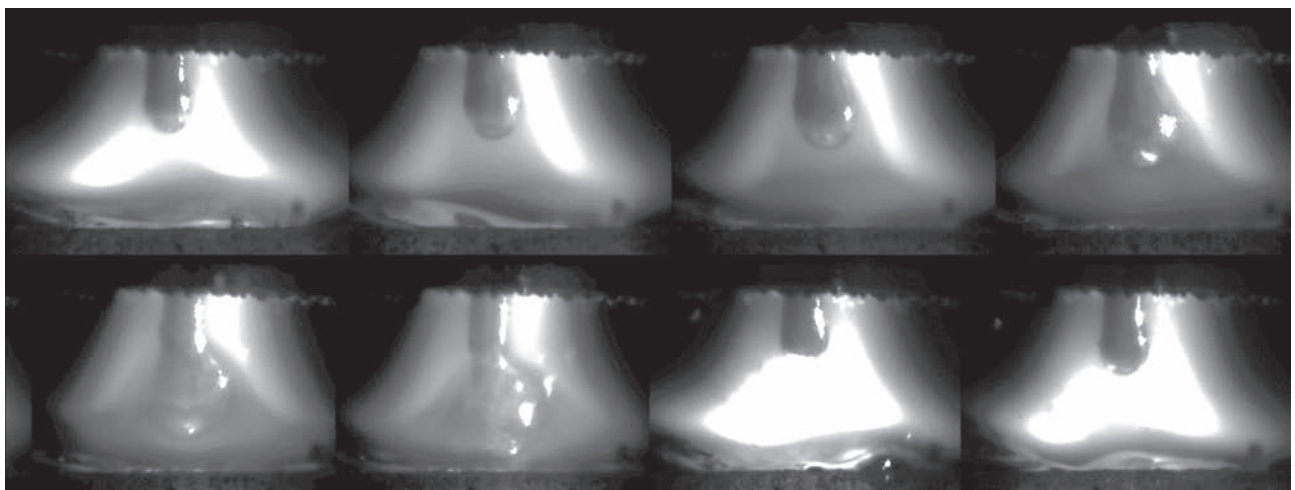
Figure 8 Successive high-speed video image of metal drop transfer during Plasma-MIG welding at a speed of 7.4 m/min, feeding wire of 1.6 mm diameter ($I_{MIG} = 165$ A, $U_{MIG} = 100$ A, time of drop transfer is about 20 ms)
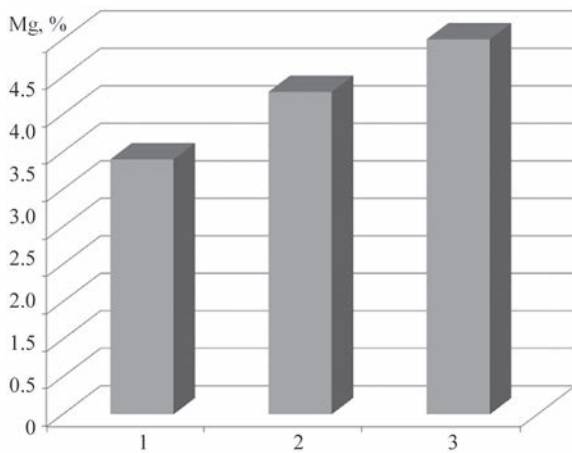
Figure 9 Averaged content of magnesium (wt.%) in metal: 1 — droplets which were formed during MIG process; 2 — droplets which were formed during Plasma-MIG process; 3 — electrode metal (ER5356)

of magnesium content). To compare the obtained results, the droplets of electrode metal obtained both by Plasma-MIG welding ($P_{\Sigma} \approx 6600$ W) and by pulsed MIG welding ($P_{MIG} \approx 6580$ W) were investigated. It was found that the porosity of the droplets obtained by pulsed MIG welding is higher than the porosity of the droplets obtained by Plasma-MIG welding. According to the results of spectral investigations, the content of magnesium in the conglomerate droplets of the electrode metal was determined (Figure 9).

In the course of investigations, cross macro- and micro-sections of welded joints were made, their metallographic analysis was performed (ISO10042:2018), and mechanical tests on static tension were performed (ISO 4136:2012). Also, the residual stress-strain state (SSS) of the welded specimens was determined [17].

The strength values of the specimens of welded joints during static tensile tests were determined by averaging the data obtained on three specimens with a removed root bead and on three specimens with a removed root bead and an upper weld reinforcement for the cases of pulsed MIG and Plasma-MIG welding. For the base metal, the data were averaged on two specimens of each of the alloys. As is seen from Table 4, the strength of the joints produced by Plasma-MIG welding is 80−90 % of the strength of the base metal, while the strength of the joints produced by pulsed MIG welding is 75−80 % of the strength of the base metal.

SSS of the specimens with the sizes of 320×205×5 mm of 1561 alloy with a longitudinal butt weld produced by pulsed MIG and Plasma-MIG welding were measured by the method described in [17]. The values of longitudinal f_1−f_3 and transverse Δ_1−Δ_2 deflections (respectively, at the beginning and at the end of the joint) were measured along the axes of the specimens. To provide comparability of the results, the modes were selected having similar values of input energy ($E \approx 630$ J/mm). Welding modes and geometric characteristics of the investigated specimens are presented in Table 5, and their cross-sections are similar to those shown in Figure 7, *a*, *b*.

Measurements of the component σ_x of the flat stress state were performed in three transverse weld cross-sections S_1−S_3 on the facial side of the plate (from the left edge $S_1 = 166$, $S_2 = 148$, $S_3 = 156$ mm), and in one weld transverse cross-section (from the same edge $S_5 = 168$ mm) — on the back side. Measurements of the longitudinal component σ_x of the flat stress state were performed along the axis along

Table 4 Values of strength σ_t at static tension of joints of 1561 and 5083 alloys ($\delta = 5.0$ mm), welded at a speed of 10 mm/s

Welding process/alloy	σ_t, MPa			
	specimens with removed root bead		specimens with removed root and upper beads	
	On separate specimens	Averaged values	On separate specimens	Averaged values
Pulsed-MIG welding/1561	330 334 340	335	290 283 284	286
Plasma-MIG welding/1561	348 345 342	345	308 307 302	306
Base metal/1561	–	–	380 374	377
Pulsed-MIG welding/5083	282 292 287	287	257 252 254	254
Plasma-MIG welding/ 5083	305 303 299	302	280 285 292	286
Base metal/5083	–	–	315 325	320

Table 5 Modes of pulsed MIG and Plasma-MIG welding at a speed of 10 mm/s and values of deflections of welded plates of 1561 alloy ($\delta = 5.0$ mm) (electrode wire ER5356 with a diameter of 1.6 mm)

Type of welding											
MIG					Plasma-MIG						
I_{MIG}, A	U_{MIG}, V	E_{MIG}, J/mm	$f_1/f_2/f_3$, mm	Δ_1/Δ_2	I_{MIG}, A	U_{MIG}, V	I_{PL}, A	U_{PL}, V	E_Σ, J/mm	$f_1/f_2/f_3$, mm	Δ_1/Δ_2
240	26.5	636	1.0/1.5/1.2	1.5/1.5	150	25.5	100	24.6	629	−0.3/−0.5/−0.4	−0.5/−0.5

the welds: from the facial side in the cross-section S_4, on the back side — in the cross-section S_6 of the weld. Duplication of σ_x measurements on the facial and back side of the plate were performed to provide reliability of the results. The values of the transverse component σ_y were recorded only on the facial side in the cross-section S_3.

Analysis of the specimen produced by pulsed MIG welding (Table 5, Figure 6, *a*) showed the presence of longitudinal deflections f_1–f_3 in the range of values of 1.0−1.5 mm, directed away from the facial surface. The values of the transverse deflections Δ_1–Δ_2 are stable along the length of the

welded joint and are 1.5 mm. The peculiarities of these changes in the shape of the specimen are determined by the shape of the weld penetration (Figure 6, *a*), which is characterized by the discrepancy between the line of applying shrinkage shortening and the neutral cross-sectional axis. The result of this discrepancy is the appearance of a bending moment that causes deformation of the plate in the longitudinal direction. The stability of the values Δ along the length of the plate is associated with its geometric characteristics that provide a uniform heat removal from the surface during the welding thermodeformational cycle.

Table 6 Distribution of residual welding stresses on the facial and back sides of the plates 1561 ($\delta = 5.0$ mm), welded by pulsed MIG and Plasma-MIG methods
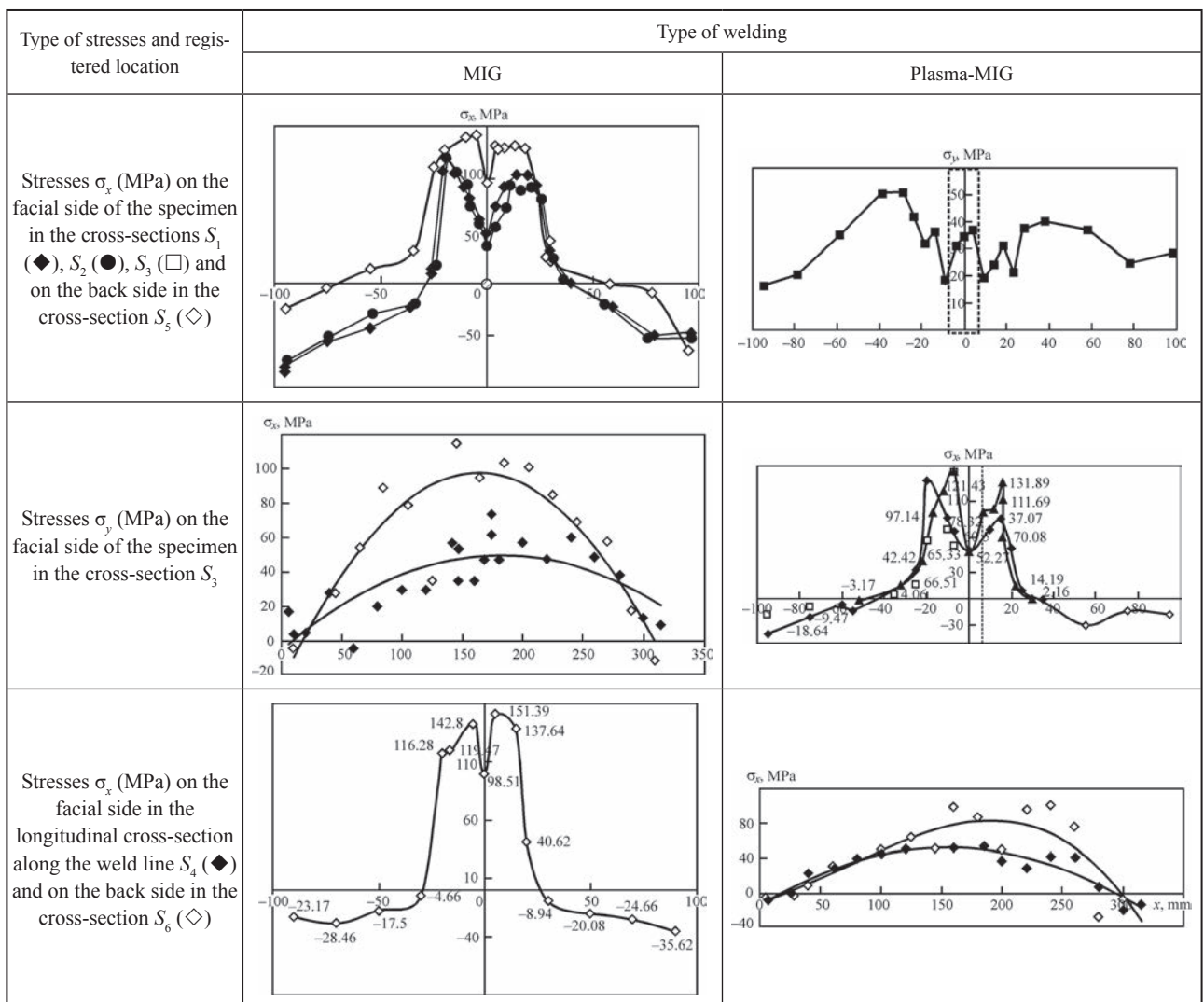
In the case of pulsed MIG welding in the center of the weld on the facial and back surfaces of the plate there is a local reduction in tensile stresses σ_x to $+45-+50$ and 100 MPa, respectively (Table 6, MIG). The peak values σ_x on the facial and back surfaces of the plate take place in the fusion zone and reach 100 and 140 MPa, respectively. The reactive compressive stresses σ_x on the facial and back surfaces reach the maximum values on the longitudinal edges of the plate $-50- -80$ and $-25- -60$ MPa, respectively. Such a form of the diagram of compressive stresses σ_x is associated with a small width of the plate, at which the stresses in the cross-section do not reach zero values. When comparing the diagrams σ_x on both sides of the plate, it can be seen that there is a significant bending component of stresses, which confirms the obtained shape of the specimen deformation.

Estimation of the transverse component of tensile stresses σ_y showed that its level is much lower than the level of stresses σ_x and does not exceed 40–50 MPa, and the sign of stresses is not changed along the measured cross-section (Table 6, MIG). Moreover, there is a local decrease in σ_y on the fusion line, and the peak values of stresses correspond to the zones of cross-section at a distance of $30-40$ mm from the center of the weld.

The distribution of residual longitudinal stresses in the welded plate along the weld line confirms the results obtained for the transverse cross-section S_1 (Table 6, MIG). The diagrams of σ_x on both sides of the plate are characterized by a difference in peak values, which determines the significant bending component of the stress-strain state of the plate and confirms the nature of its change of shape.

Analysis of the performed Plasma-MIG welding of the specimen (Table 5, Figure 7, b) showed the presence of longitudinal deflections f_1-f_3 with the values of $-0.3- -0.5$ mm, directed towards the facial surface. The values of transverse deflections $\Delta_1-\Delta_2$ are stable along the length of the welded joint and are also at the level of 0.5 mm. The peculiarities of this change of shape are determined by the shape of the weld (Figure 7, b), which is characterized by the practical coincidence of the line of applying the shrinkage shortening and the neutral axis of the weld cross-section. Comparison of the shapes of the welds in Figure 7, a and Figure 7, b shows that the cross-sectional area of the weld in Plasma-MIG welding is by ~ 30 % smaller than in pulsed MIG welding. The plate produced by Plasma-MIG welding is characterized by smaller longitudinal shrinkage shortenings of the weld metal and, accordingly, a lower value of the bending moment than the specimen after pulsed MIG welding. This fact explains the decrease (up to three times) in the value of deformation in the longitudinal direction of the plate produced by Plasma-MIG welding. Morever, the stability and low values associated with the shape of the weld Δ is characterized by a more uniform (as compared to pulsed MIG welding) penetration through the thickness of the plate, as well as geometric characteristics of the specimen, which provide a stable heat removal from the surfaces during the welding thermodeformational cycle.

The distribution of residual longitudinal stresses σ_x in the transverse cross-sections of the welded plate after Plasma-MIG welding is presented in Table 6 (Plasma-MIG). In the center of the weld on the facial and back surfaces of the plate there is a local decrease in tensile stresses up to $45-50$ and 100 MPa, respectively. The peak values σ_x on the facial and back surfaces take are located in the fusion zone and reach 140 and 150 MPa, respectively. Reactive compressive stresses σ_x on the facial and back surfaces reach maximum values of $-20- -40$ MPa on the longitudinal edges of the plate. This shape of the diagram σ_x like in the case of pulsed MIG welding, is associated with a small width of the plate, at which the compressive stresses in the transverse cross-section do not reach zero values. When comparing the diagrams σ_x on both sides of the plate, it can be seen that, in contrast to pulsed MIG welding, the bending stress component in the reactive zone of the diagram is insignificant, which determines a lower value of the specimen deformation.

The distribution of residual longitudinal stresses σ_x in the welded plate along the weld line confirms the results obtained for the transverse cross-section S_1 (Table 6, Plasma-MIG). The diagrams σ_x on both sides of the plate produced by Plasma-MIG welding are characterized by a smaller difference in peak values than in pulsed MIG welding, which determines the bending component of the stress-strain state of the plate and confirms the characteristics of its change of shape (Table 5).

In the course of the carried out work, a number of technological experiments with Plasma-MIG welding was performed, which showed that with an increase in the thickness of butt-welded plates, the efficiency of using this method increases. This is associated with the lack of need to perform preparation of edges to be joined during welding plates with a thickness of $\delta \leq 8$ mm and a small angle (15°) of the development for $\delta = 10$ mm, as well as lower electrode wire consumption as compared to MIG welding. If during welding of plates with a thickness of $\delta = 5$ mm, this reduction in wire consumption is $10-15$ %, then at $\delta = 8$ mm it is $20-25$ %, and at $\delta = 10$ mm it is up to 30 %, which is predetermined first of all by eliminating or minimizing preparation of edges.

Analysis of the parameters of pulsed MIG welding and hybrid Plasma-MIG welding of plates from the considered aluminium alloys, as well as sizes of the produced welds, showed that the use of Plasma-MIG welding allows reducing the weld width by 20−25 %. Moreover, the amount of input energy is reduced to 25 %, which has a positive effect on strength values of the welded joint.

The mutual influence of the plasma-arc and the arc of the consumable electrode during Plasma-MIG welding is mainly expressed in the fact that the former compresses the latter, preventing spattering of the electrode metal and providing a concomitant heating of the welded edges. This allows the constricted arc of the consumable electrode to weld a much greater thickness of the metal than a traditional open arc. In addition, the plasma-arc helps to eliminate undercuts and create a smoother transition from the upper bead to the base metal. An increase in voltage on the arc of the nonconsumable electrode predicted in [12] with an increase in the consumption of plasma-forming gas (from 5 to 25 l/min) was confirmed in practice and amounted to about 1−2 V, which is not a quite significant index, but in general has a positive effect on weld formation.

The study of electrode metal droplets formed during Plasma-MIG welding showed an improvement in the results as compared to traditional MIG welding. It can be assumed that a decrease in the total volume of voids (porosity) in the droplets obtained during Plasma-MIG welding is caused by reducing the diameter of the arc column of the consumable electrode, which occurs under the influence of the plasma-arc, as well as improving the conditions of arc breakdown in the area of droplets transfer. The latter, unlike the process of a pulsed MIG welding, allows the active spot of the arc to be more uniformly distributed along the perimeter of the droplet under the conditions of a lower heat input. All these factors promote the reduction of boiling of the liquid drop, evolutiuon of hydrogen and reducing the evaporation of easily boiling magnesium. As a result, the content of magnesium is increased by 15−25 %, growing from 60−70 % in the MIG process to 80−85 % in the Plasma-MIG process.

When analyzing the residual stress state of the plates welded by pulsed MIG and Plasma-MIG methods, it is possible to note some discrepancy between the level of tensile stresses and the values of deflections. Thus, the peak values of tensile stresses σ_x for these welding methods, in contrast to the values of deflections, are quite close, as well as the values of the bending component of stresses in the active zone (in the center of the weld). This fact can be explained by a low longitudinal rigidity of the studied welded plates, as well as by the peculiarities of stress-strain states, which are set by pulsed MIG and Plasma-MIG welding. The diagrams σ_x in the reactive stress zone go to the free longitudinal edges. The stresses at the edges of the plate during Plasma-MIG welding are significantly lower than during pulsed MIG welding, which reduces the longitudinal deflections and, accordingly, increases the level of tensile stresses σ_x. Thus, the level of stresses σ_x in the bent plate after pulsed MIG welding can be compared with the level σ_x in a flat plate after Plasma-MIG welding. These observations to some extent coincide with the conclusions given in [18, 19]. It can be concluded that when comparing the stress states of the plates with equal values of deflections made by Plasma-MIG and pulsed MIG welding, the values σ_x in the latter will be higher.

Conclusions

1. To improve the mechanical properties and reduce the values of stress-strain state of welded joints of alloyed aluminium alloys, technological methods of hybrid Plasma-MIG welding were proposed, which as compared to the traditional MIG process allow reducing the electrode wire consumption by 10−30 %, input energy by up to 25 %, residual deformations by 2−3 times, residual stresses by ~ 20 % according to the absolute value and reducing the burnout of such alloying element as Mg by 15−20 %.

2. It was established that a constricted plasma-arc of reverse polarity, which has a power exceeded by 20−30 %, reduces the size of the arc of the consumable electrode, deepens it into the weld metal, allows obtaining a vapour-gas channel of the specimen without a keyhole formation, improves weld formation and reduces the tendency to formation of inner pores and lacks of fusion.

3. It was established that during hybrid Plasma-MIG welding of aluminium 1561 and 5083 alloys of up to 10 mm thickness at the speeds of 30−60 m/h the integrated input energy is $E_\Sigma = 500−1000$ J/mm, which has a positive effect on the composition and structure of the weld, providing the strength of the joints at the level of 80−90 % of the base metal, unlike the strength of 75−80 % during pulsed MIG welding.

● *No.2017GDASCX-0411* «*Capacity-Building of Innovation-Driven Development for Special Fund Projects*», *Guangdong Academy of Sciences (China)*;

● *No.2018A050506058* «*Research and application of hybrid laser and arc welding technology with high power on high-strength steel for shipbuilding*», *Guangzhou, China.*

1. Korzhyk, V., Khaskin, V., Perepychay, A. et al. (2020) Forecasting the results of hybrid laser-plasma cutting of carbon steel. Eastern-European *J. of Enterprise Technologies*, 1/2(104), 6–15.

2. *Adrianus Christinus Henricus Jozef* Liei'kens, Wilhelmus Gerardus Essers (1971) *Method of and device for plasma-arc welding.* U.S. Philips Corporation. Pat. 3,612,807 US, Int. Cl. B23k9/00.

3. Ton, H. (1975) Physical properties of the plasma-MIG welding arc. *J. of Physics D: Applied Physics*, **8**, 922–933.

4. Matthes, K.-J., Kusch, M. (2000) *Plasma-MIG-Schweissen. Praktike*, **5**, 182–188.

5. (2007) Hybrid welding: An alternative to SAW. *Welding J.*, **0**, 42–45.

6. Shchitsyn, Yu.D., Tytkin, Yu.M. (1986) Consumable electrode plasma welding of aluminium alloys. *Svarochn. Proizvodstvo*, **5**, 1–2 [in Russian].

7. Shchitsyn, Yu.D., Shchitsyn, V.Yu., Herold, H. et al. (2003) Plasma welding of aluminium alloys. *Ibid.*, 5, 36–42 [in Russian].

8. Bai, Yan, Gao, Hong-Ming, Qiu, Ling (2010) Droplet transition for plasma-MIG welding on aluminium alloys. *Transact. Nonferrous Met. Soc. China*, **0**, 2234–2239.

9. *Tiago Vieira* da Cunha, Jair Carlos Dutra (2007) Processo Plasma-MIG — Contribuição do Arco Plasma na Capacidade de Fusão do Arame. *Soldagem Insp. São Paulo*, 12(2), 89–96.

10. Grinyuk, A.A., Korzhik, V.N., Shevchenko, V.E. et al. (2016) Hybrid technologies of welding aluminium alloys based on consumable electrode arc and constricted arc. *The Paton Welding J.*, **6**, 98–103.

11. Hee-Keun, Lee, Kwang-San, Chun, Sang-Hyeon, Park, Chung-Yun, Kang (2015) Control of surface defects on plasma-MIG hybrid welds in cryogenic aluminium alloys. *Int. J. Nav. Archit. Ocean Eng.*, **7**, 770–783.

12. Sydorets, V., Korzhyk, V., Khaskin, V. et al. (2017) On the thermal and electrical characteristics of the hybrid plasma-MIG welding process. *Mat. Sci. Forum*, **0**, 63–71.

13. Goldak, J.A., Akhlaghi, M. (2005) *Computational welding mechanics*. O., USA.

14. Bofang, Zhu. (2018) *The Finite Element Method: Fundamentals and Applications in Civil, Hydraulic, Mechanical and Aeronautical Engineering*. John Wiley & Sons Singapore Pte. Ltd.

15. Khaskin, V.Yu., Korzhyk, V.M., Peleshenko, S.Y., Wu, Boyi (2015) Evaporation of alloying elements in the material to be welded using laser radiation. *Pervyi Nezavisimyi Nauchnyi Vestnik,* **3**, 108–114.

16. Wang, J., Nishimura, H., Katayama, S., Mizutani, M. (2011) Evaporation phenomena of magnesium from droplet at welding wire tip in pulsed MIG arc welding of aluminium alloys. *Sci. Technol. Weld. Join.*, **6**, 418–425.

17. Lobanov, L.M., Pivtorak, V.A., Savitsky, V.V., Tkachuk, G.I. (2006) Procedure for determination of residual stresses in welded joints and structural elements using electron speckle-interferometry. *The Paton Welding J.*, **1**, 24–29.

18. Korzhik, V.N., Pashchin, N.A., Mikhoduj, O.L. et al. (2017) Comparative evaluation of methods of arc and hybrid plasma-arc welding of aluminium alloy 1561 using consumable electrode. *Ibid.*, **4**, 32–37.

19. Korzhyk, V.N., Kvasnytskyi, V.V., Khaskin, V.Yu. (2017) Influence of rigid restraint on formation of residual stress-strain state of plate butt joints from 1561 alloy in MIG, PAW and hybrid PAW-MIG welding. *American Scientific J.*, 17(1), 14–29.